Fermi surface nesting induced strong pairing in iron-based superconductors

K. Terashima[1], Y. Sekiba[2], J. H. Bowen[3], K. Nakayama[2], T. Kawahara[2], T. Sato[2,4], P. Richard[5], Y.-M. Xu[6], L. J. Li[7], G. H. Cao[7], Z.-A. Xu[7], H. Ding[3], and T. Takahashi[2,5]

[1]*UVSOR Facility, Institute for Molecular Science, Okazaki 444-8585, Japan*

[2]*Department of Physics, Tohoku University, Sendai 980-8578, Japan*

[3]*Beijing National Laboratory for Condensed Matter Physics, and Institute of Physics, Chinese Academy of Sciences, Beijing 100190, China*

[4]*TRIP, Japan Science and Technology Agency (JST), Kawaguchi 332-0012, Japan*

[5]*WPI Research Center, Advanced Institute for Materials Research, Tohoku University, Sendai 980-8577, Japan*

[6]*Department of Physics, Boston College, Chestnut Hill, MA 02467, USA*

[7]*Department of Physics, Zhejiang University, Hangzhou 310027, China*

The discovery of high-temperature superconductivity in iron pnictides[1-4] raised the possibility of an unconventional superconducting mechanism in multiband materials. The observation of Fermi-surface(FS)-dependent nodeless superconducting gaps[5-7] suggested that inter-FS interactions may play a crucial role in superconducting pairing[8-11]. In the optimally hole-doped $Ba_{0.6}K_{0.4}Fe_2As_2$, the pairing strength is enhanced simultaneously ($2\Delta/T_c$~7) on the nearly nested FS pockets, *i.e.* the inner holelike (α) FS and the two hybridized electronlike FSs, while the pairing remains weak ($2\Delta/T_c$~3.6) in the poorly-nested outer hole-like (β) FS[5,12]. Here we report that in the electron-doped $BaFe_{1.85}Co_{0.15}As_2$ the FS nesting condition switches from the α to the β FS due to the opposite size changes for hole- and electron-like FSs upon electron doping. The strong pairing strength ($2\Delta/T_c$~6) is also found to switch to the nested β FS, indicating an intimate connection between FS nesting and superconducting pairing, and strongly supporting the inter-FS pairing mechanism in the iron-based superconductors.

In charge doped superconductors, such as copper oxides (cuprates), electron or hole doping may influence the superconducting (SC) properties differently[13,14]. As an example, angle-resolved photoemission spectroscopy[15] (ARPES) and Raman scattering[16] revealed a non-monotonic behaviour in the SC gap function of the electron-doped cuprates which is different from the simple $d_{x^2-y^2}$-wave function observed in the hole-doped cuprates[17]. On the other hand, in the new Fe-based superconductors, no direct comparison of the SC order parameter has been made between hole- and electron-doped systems. ARPES studies on hole-doped $Ba_{1-x}K_xFe_2As_2$ have observed isotropic gaps that have different values on different Fermi surfaces (FSs) with strong pairing occurring on the nearly nested FS pockets[5,7]. Thus, it is particularly important to conduct a comparison of the SC gaps and their FS dependence of an electron-doped pnictide. We have chosen $BaFe_{1.85}Co_{0.15}As_2$, which is electron doped[18] and has the same crystal structure as the $Ba_{1-x}K_xFe_2As_2$ system[4].

Figures 1a and 1b show ARPES intensity plots of $BaFe_{1.85}Co_{0.15}As_2$ (T_c = 25.5 K) as a function of binding energy and momentum (k) along two high symmetry lines in the Brillouin zone (BZ). We observe a holelike dispersion centred at the Γ point and two electronlike FSs near the M point. Even though a reasonable agreement is found between experiment and renormalized band calculations[19], some experimental features such as the energy position of the 0.2 eV band at the Γ point and the bottom of the electron band at the M point, are not well reproduced by band calculations. This suggests a possible orbital and k-dependence of the mass-renormalization factor. Figure 1c shows the ARPES intensity at the Fermi level (E_F) plotted as a function of the in-plane wave vector.

A circular and an elongated intensity pattern centred at the Γ and M points are clearly visible, and they are attributed to the hole- and electron-like bands in Figs. 1a and 1b. In Figures 1d and 1e, we show ARPES intensity plots near E_F and the corresponding energy distribution curves (EDCs) measured at three representative cuts indicated in Fig. 1c. In cut 1 of Fig. 1e, two holelike bands are clearly visible. The inner band, assigned to the α band[5], sinks significantly (~30 meV) and does not create a small FS pocket as observed in the hole-doped samples[5], confirming the electron doping by the Co substitution. The outer band (the β band) crosses E_F creating a hole pocket at the Γ point. Along cut 3 which is close to M, we can distinguish an electronlike band crossing E_F with a bottom at ~40 meV creating an elongated FS pocket shown in Fig. 1c. A closer look at the second derivative of momentum distribution curves (MDCs) in Fig. 1f reveals the presence of an additional band whose dispersion near E_F is nearly parallel to the main band. This suggests that the electronlike FSs consist of the inner (γ) and outer (δ) pockets resulting from the hybridization of two ellipsoidal pockets elongated along the k_x and k_y directions[20] (see Fig. 1c). More significantly, the β hole pocket is nearly nested with the electron pockets, in sharp contrast to the observation of a good FS nesting between the α hole pocket and the electron pockets in the hole-doped $Ba_{0.6}K_{0.4}Fe_2As_2$.

We now illustrate how the SC gap evolves below T_c on each FS. Figure 2a displays the temperature (T) dependence of the EDCs at a Fermi vector (k_F) on the β hole pocket measured across T_c. At 8 K, the midpoint of the leading edge below T_c is apparently shifted toward higher binding energy by ~4 meV with a pile-up of spectral weight at ~7 meV, indicating the opening of a

SC gap. We have eliminated the effect of the Fermi-Dirac distribution function by symmetrizing the EDCs at each temperature[21] (Fig. 2b). To cancel out the influence of the V-shaped spectral density of states (DOS), which originates from the tail of the α band, we divided each symmetrized spectrum by the 33-K spectrum (see top of Fig. 2b). As one easily notices, a sharp coherence peak emerges below T_c at 7 meV. Interestingly, the spectral weight at E_F displays a small depression even at T = 27 K, indicating a possible weak pseudogap just above T_c. We have estimated the size of the SC gaps and plotted them in Fig. 2c. It is found that the simple Bardeen-Cooper-Schrieffer mean-field T-dependence with $\Delta(0)$ = 7 meV reproduces satisfactorily the extracted gap amplitudes. In Figures 2d and 2e, we plot the T-dependence of raw and symmetrized EDCs measured on the ellipsoidal electron pocket. Although the overall T-dependence of the leading-edge shift and the spectral weight suppression below T_c on the electron pockets are qualitatively similar to those of the β FS, there are some essential differences: a weaker coherence-peak weight accompanied with a reduction of spectral weight at E_F, and a smaller SC-gap size (4.5 *vs*. 6.7 meV; see Fig. 2f) are observed. These results demonstrate the FS-sheet dependence of the SC gap. We also noticed that the weight of the coherence peak is much weaker than that of hole-doped $Ba_{0.6}K_{0.4}Fe_2As_2$ (Ref. 5), possibly owing to a lower superfluid density due to a lower T_c value (25.5 *vs*. 37 K) and disorder scattering induced by in-plane Co substitution.

Next we turn our attention to the k-dependence of the SC gaps. Figures 3a and 3b show the symmetrized EDCs measured at 8 K at various k_F points on (a) the β hole pocket and (b) the ellipsoidal electron pocket. As shown in Fig.

3d, the SC gap of each FS is nearly constant, indicating an isotropic *s*-wave nature. On the other hand, the average gap values of the hole and electron pockets are different (6.6 and 5.0 meV, respectively), establishing unambiguously the FS-dependent nature of the SC gap.

A direct comparison of the ARPES data on the electron- and hole-doped SC pnictides allows us to conclude that: (i) the SC gap opens on multiple FSs centred at the Γ and M points, (ii) the SC gap is nodeless and exhibits nearly isotropic behaviour on each FS, and (iii) the pairing strength, as reflected by the ratio of $2\Delta/k_BT_c$, is related to the FS nesting condition between the electron and hole pockets. In hole-doped $Ba_{0.6}K_{0.4}Fe_2As_2$ (Ref. 5,12), the interband scattering via the wavevector $Q\sim(\pi,0)$ (as defined in the unreconstructed BZ) has been suggested to enhance the pairing amplitude of the α and γ(δ) FSs, resulting in large $2\Delta/k_BT_c$ values of 7.2-7.7, while the poorly-nested β FS has a value of 3.6, close to the weak-coupling regime. Remarkably, in electron-doped $BaFe_{1.85}Co_{0.15}As_2$, the β (but not α) and γ(δ) FSs are also connected by the same $Q\sim(\pi,0)$ and possess strong-coupling $2\Delta/k_BT_c$ values of 5.9 and 4.5, respectively, suggesting an enhancement of the pairing amplitude due to similar interband scattering on the nearly nested FSs. The observation that the pairing strength in the β band increases from 3.6 in the optimally hole-doped sample to 5.9 in the optimally electron-doped sample strongly suggests that the SC coupling strength is more related to the nesting condition among the FSs than to the orbital characters themselves. All these facts suggest the inter-pocket scattering as the main pairing mechanism in the pnictides.

At this point, a few essential issues regarding the nature of the

unconventional pairing mechanism need to be addressed. The first one is the cause of a small difference in the SC gap size of the observed FSs in the electron-doped system. This may be related to the difference in the partial DOS between electron and hole pockets. The existence of two electron pockets would give rise to a larger DOS at E_F in the electron pockets than in the hole pocket. This leads to a relative enhancement of the pairing amplitude in the hole pocket due to stronger $Q\sim(\pi, 0)$ scattering from the electron pockets[22]. The second issue concerns the smaller $2\Delta(0)/k_BT_c$ values obtained on the well nested FSs in the electron-doped $BaFe_{1.85}Co_{0.15}As_2$ (4.5-5.9) as compared to the hole-doped $Ba_{0.6}K_{0.4}Fe_2As_2$ (7.2-7.7 (Ref. 5)). This might be linked to the larger pairing-breaking disorder scattering caused by the in-plane Co substitution as compared to the off-plane K substitution in $Ba_{0.6}K_{0.4}Fe_2As_2$. The last issue, which might be the most unusual, is the lack of anisotropy in the gap function on a given FS. Strictly speaking, the interband scattering condition *via* $Q = (\pi, 0)$ is not perfect in either the hole or the electron-doped systems since the shape of the hole and electron pockets does not match completely (*e.g.* see Fig. 1c). One might therefore expect a large anisotropy in the SC gap size near the M point, while the observed SC gap size is merely dependent on the FS sheet. This implies that there might be a novel mechanism that keeps the intraband SC gap constant. Our observation of isotropic SC gaps that depend on FS nesting conditions is an important step toward the full understanding of high-T_c superconductivity in iron pnictides.

Methods

High-quality single crystals of $BaFe_{1.85}Co_{0.15}As_2$ were grown by the self flux method, the same growth method as for $BaFe_{2-x}Ni_xAs_2$ (Ref. 23). From electrical resistivity measurements, T_c of the sample has been estimated to be T_c^{mid} = 25.5 K. The starting material (nominal composition) was $BaFe_{1.8}Co_{0.2}As_2$, while the actual Co content was determined by energy-dispersive X-ray spectroscopy. ARPES measurements were performed using a VG-SCIENTA SES2002 spectrometer with a high-flux discharge lamp and a toroidal grating monochromator. We have measured ARPES spectra with the He Iα resonance line (21.218 eV). The energy resolution was set at 4 and 15 meV for the measurement of the SC gap and the valence band dispersion, respectively. The angular resolution was set to 0.2°. Clean surfaces for ARPES measurements were obtained by *in-situ* cleaving of crystals in a working vacuum better than $5x10^{-11}$ Torr. The Fermi level of samples was referenced to that of a gold film evaporated onto the sample substrate. Mirror-like sample surfaces were found to be stable without obvious degradation for the measurement period of 3 days. To extract the carrier number from the ARPES measurement, we have estimated the FS volume of the β pocket and the ellipsoidal electron pocket to be 1.6% and 3.2% of the unfolded first BZ respectively. The deduced total carrier number of 0.05 electrons/Fe is close to but slightly lower than the expected value of 0.075 electrons/Fe in $BaFe_{1.85}Co_{0.15}As_2$. The small difference may suggest a possible deviation of the Co valency from 3+ and/or the finite three dimensionality of the band structure[8,24-26].

References

1. Kamihara, Y., Watanabe, T., Hirano, M. & Hosono, H. Iron-based layered supeconductor La[$O_{1-x}F_x$]FeAs (x = 0.05-0.12) with T_c = 26 K. *J. Am. Chem. Soc.* **130,** 3296-3297 (2008).

2. Takahashi, H. *et al.* Superconductivity at 43 K in an iron-based layered compound $LaO_{1-x}F_xFeAs$. *Nature* **453,** 376-378 (2008).

3. Chen, X. H. *et al.* Superconductivity at 43 K in $SmFeAsO_{1-x}F_x$. *Nature* **453,** 761-762 (2008).

4. Rotter, M., Tegel, M. & Johrendt, D. Superconductivity at 38 K in the iron arsenide $(Ba_{1-x}K_x)Fe_2As_2$. *Phys. Rev. Lett.* **101,** 107006 (2008).

5. Ding, H. *et al.* Observation of Fermi-surface-dependent nodeless superconducting gaps in $Ba_{0.6}K_{0.4}Fe_2As_2$. *Europhys. Lett.* **83,** 47001 (2008).

6. Liu, C. *et al.* K-doping dependence of the Fermi surface of the iron-arsenic $Ba_{1-x}K_xFe_2As_2$ superconductor using angle-resolved photoemission spectroscopy. *Phys. Rev. Lett.* **101**, 177005 (2008).

7. Zhao, L. *et al.* Unusual superconducting gap in (Ba,K)Fe_2As_2 superconductor. *Chin. Phys. Lett.* (in press); Preprint at <http://arxiv.org/abs/0807.0398> (2008).

8. Mazin, I. I., Singh, D. J., Johannes, M. D. & Du, M. H. Unconventional superconductivity with a sign reversal in the order parameter of $LaFeAsO_{1-x}F_x$. *Phys. Rev. Lett.* **101,** 057003 (2008).

9. Kuroki, K. *et al.* Unconventional pairing originating from the disconnected Fermi surfaces of superconducting $LaFeAsO_{1-x}F_x$. *Phys. Rev. Lett.* **101,** 087004 (2008).

10. Wang, F. *et al.* A numerical renormalization group study of the

superconducting and spin density wave instabilities in a two-band model of $MFeAsO_{1-x}F_x$ compounds. Preprint at <http://arxiv.org/abs/0805.3343v3> (2008).

11. Seo, K., Bernevig, B. A. & Hu, J. Pairing symmetry in a two-orbital exchange coupling model of oxypnictides. *Phys. Rev. Lett.* **101,** 206404 (2008).

12. Nakayama, K. *et al.* Superconducting-gap symmetry of $Ba_{0.6}K_{0.4}Fe_2As_2$ studied by angle-resolved photoemission spectroscopy. Preprint at <http://arxiv.org/abs/0812.0663v1> (2008).

13. Damascelli, A., Hussain, Z. & Shen, Z.-X. Angle-resolved photoemission studies of the cuprate superconductors. *Rev. Mod. Phys.* **75,** 473-541 (2003).

14. Campuzano, J. C., Norman, M. R. & Randeria, M. *The Physics of Superconductors* Vol. II 167-273 (Springer, Berlin, 2004).

15. Matsui, H. *et al.* Direct observation of a nonmonotonic $d_{x^2-y^2}$-wave superconducting gap in the electron-doped high-T_c superconductor $Pr_{0.89}LaCe_{0.11}CuO_4$. *Phys. Rev. Lett.* **95,** 017003 (2005).

16. Blumberg, G. *et al.* Nonmonotonic $d_{x^2-y^2}$ superconducting order parameter in $Nd_{2-x}Ce_xCuO_4$. *Phys. Rev. Lett.* **88,** 107002 (2002).

17. Ding, H. *et al.* Angle-resolved photoemission spectroscopy study of the superconducting gap anisotropy in $Bi_2Sr_2CaCu_2O_{8+x}$, *Phys. Rev. B* **54**, R9678 (1996).

18. Sefat, A. S. *et al.* Superconductivity at 22 K in Co-doped $BaFe_2As_2$ crystals. *Phys. Rev. Lett.* **101,** 117004 (2008).

19. Xu, G., Zhang, H., Dai, X. & Fang, Z. Electron-hole asymmetry and quantum critical point in hole-doped $BaFe_2As_2$. Preprint at

<http://arxiv.org/abs/0807.1401v1> (2008).

20. Ding, H. *et al*. Electronic structure of optimally doped pnictide $Ba_{0.6}K_{0.4}Fe_2As_2$: a comprehensive ARPES investigation. Preprint at <http://arxiv.org/abs/0812.0534v1> (2008).

21. Norman M. R. *et al*. Destruction of the Fermi surface in underdoped high Tc superconductors. *Nature* **392**, 157-160 (1998).

22. Dolgov, O. V., Mazin I. I., Parker, D., and Golubov, A. A. Interband superconductivity: contrasts between BCS and Eliashberg theory. Preprint at <http://arxiv.org/abs/0810.1476v1> (2008).

23. Li, L. J. *et al*. Superconductivity induced by Ni doping in $BaFe_2As_2$. Preprint at <http://arxiv.org/abs/0809.2009v1> (2008).

24. Singh, D. J. Electronic structure and doping in $BaFe_2As_2$ and LiFeAs: Density functional calculations. *Phys. Rev. B* **78,** 094511 (2008).

25. Nekrasov, I. A. Pchelkina, Z. V. & Sadovskii, M. V. Electronic structure of prototype AFe_2As_2 and ReOFeAs high-temperature superconductors: a comparison. Preprint at <http://arxiv.org/abs/0806.2630> (2008).

26. Gordon, R. T. *et al*. Unconventional London penetration depth in $Ba(Fe_{0.93}Co_{0.07})_2As_2$ single crystals. Preprint at <http://arxiv.org/abs/0810.2295> (2008).

Acknowledgments

We thank X. Dai, Z. Fang, and Z. Wang for providing their LDA results and valuable discussions. K. T. and K. N. thank JSPS for financial support. This work was supported by grants from JSPS, TRIP-JST, CREST-JST, MEXT of Japan, the Chinese Academy of Sciences, NSF, Ministry of Science and Technology of China, and NSF of US.

Competing Interests Statement

We have no competing financial interests.

Correspondence and requests for materials should be addressed to K.T. (e-mail: kensei@ims.ac.jp).

Figure legends

FIG. 1(COLOUR)

Fermi surface and band structure of an electron-doped $BaFe_{1.85}Co_{0.15}As_2$.

a,**b**, ARPES intensity plots of $BaFe_{1.85}Co_{0.15}As_2$ (T_c = 25.5 K) as a function of wave vector and binding energy measured at 8 K along **a** the ΓX and **b** the ΓM lines with the He Iα ($h\nu$ = 21.218 eV) resonance line, together with the band dispersion from the first-principle calculations for k_z = 0 and π (blue and red curves, respectively). Calculated bands for $BaFe_2As_2$ (Ref. 19) were shifted downward by 40 meV and then renormalized by the factor of 2. Green broken lines in **a** and **b** denote the expected E_F positions of $BaFe_2As_2$ and $Ba_{0.6}K_{0.4}Fe_2As_2$. **c**, FS contour determined by plotting the ARPES spectral intensity integrated within ±5 meV with respect to E_F. Black circles in **c** show determined k_F positions, while gray circles are the symmetrized k_F points by assuming the four-fold symmetry with respect to the Γ and M point, respectively. **d**, ARPES spectral intensity at 8 K as a function of wave vector and binding energy, and **e** corresponding EDCs measured along three representative cuts 1-3 shown in **c**. Circles in **e** traces the energy dispersion of the α and β bands. **f**, Second derivative plot of MDCs along cut 3 to highlight the presence of another weaker electronlike band (δ).

FIG 2 (COLOUR)

Temperature dependence of the superconducting gap.

a, *T*-dependence of EDC measured at a k_F point on the β FS (red dot in inset). **b**, Symmetrized EDCs and the same but divided by the spectra at T = 33 K.

Dashed line denotes the position of SC coherence peak. **c**, *T*-dependence of the SC gap size. Solid line is the BCS mean-field gap with T_c = 25.5 K and $\Delta(0)$ = 7 meV. **d-f**, same as **a-c**, but measured on the k_F point of the ellipsoidal electron pocket. Dashed line in **f** is the same as the solid line in **c**.

FIG. 3(COLOUR)

Momentum dependence of the superconducting gap.

a,**b**, Symmetrized EDCs at 8 K measured at various k_F points on the β and electronlike FS, labelled by respective coloured symbols correspondingly. **c**, Extracted FS from the ARPES measurements together with the definition of FS angle (θ). **d**, SC gap values at 8 K as a function of θ extracted from the EDCs shown on the polar plot, for the β and electronlike FSs (red and blue dots, respectively). Dashed circles represent the averaged gap value.

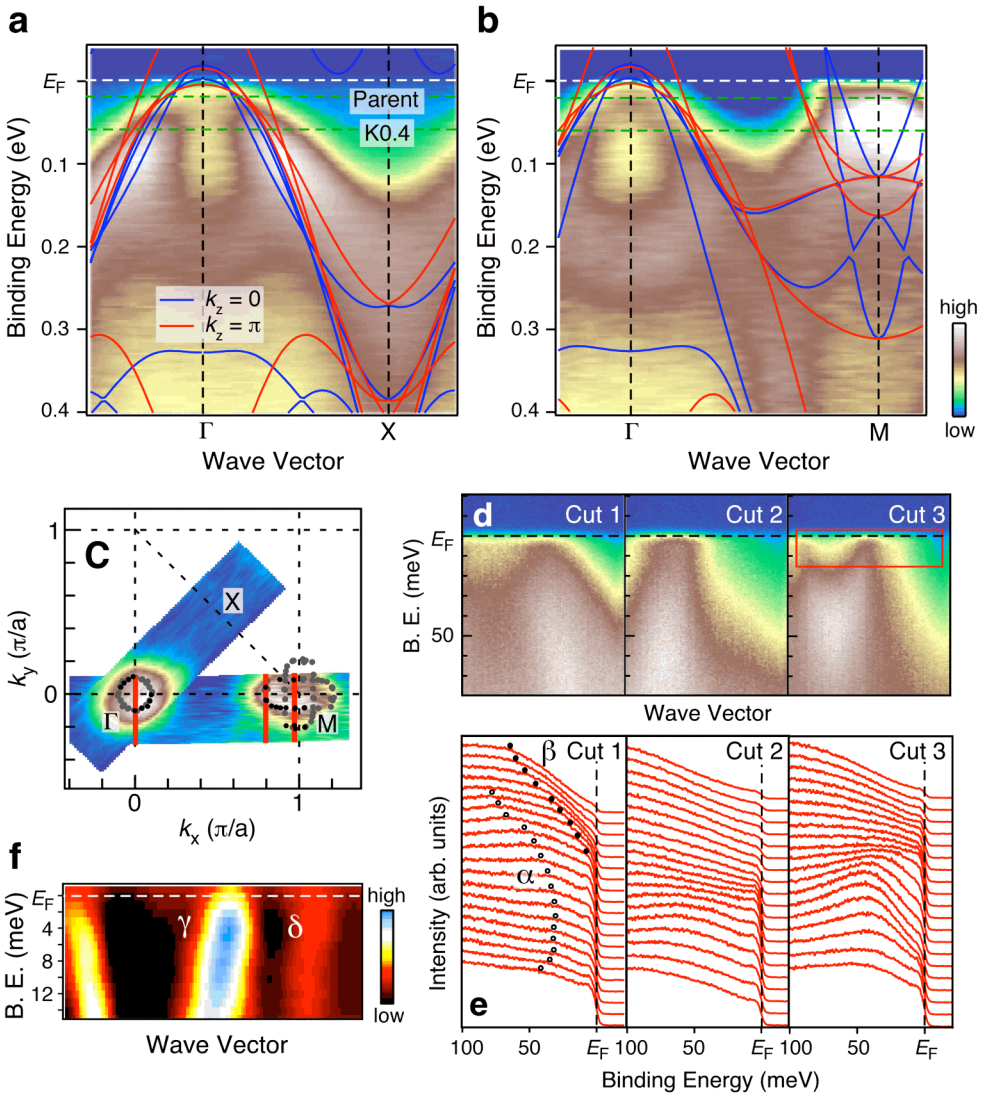
a
b
Parent
K0.4
E_F
Binding Energy (eV)
0.1
0.2
0.3
0.4
$k_z = 0$
$k_z = \pi$
Γ
X
M
Wave Vector
high
low
C
k_y (π/a)
k_x (π/a)
d
Cut 1
Cut 2
Cut 3
B. E. (meV)
50
e
β
α
Intensity (arb. units)
100
Binding Energy (meV)
f
γ
δ
4
8
12

Figure 1

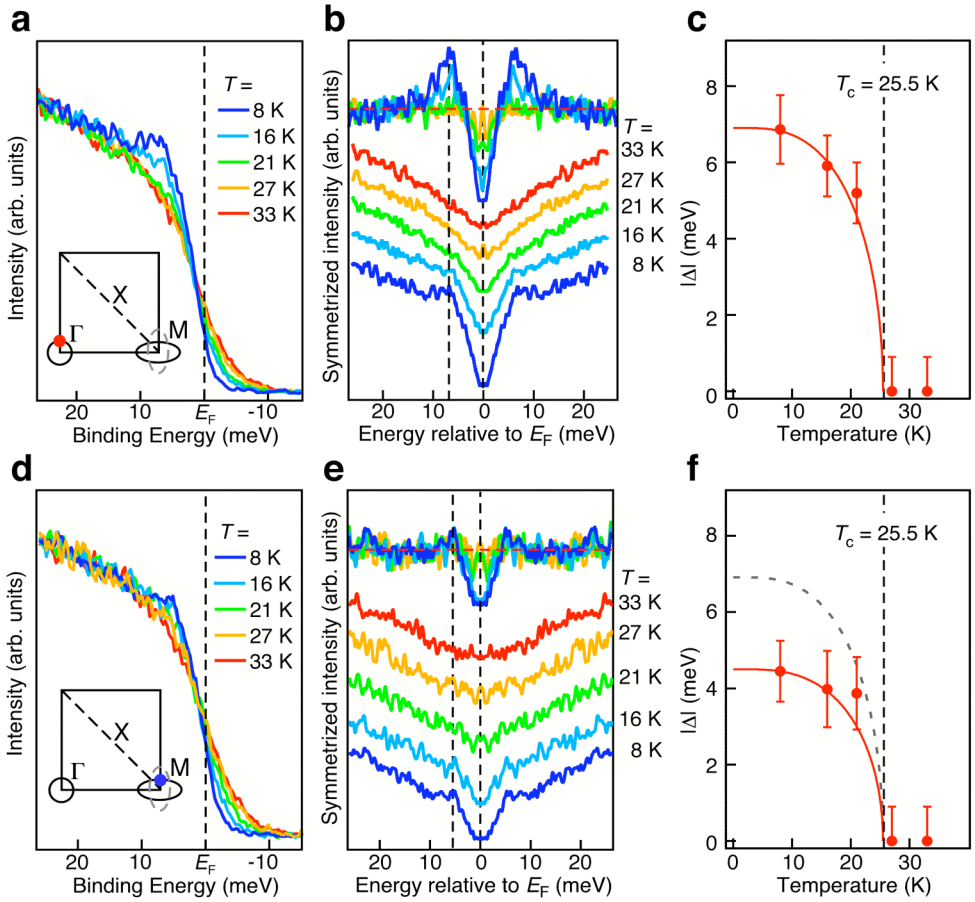
a
b
c
d
e
f
Intensity (arb. units)
Binding Energy (meV)
T =
8 K
16 K
21 K
27 K
33 K
Γ
X
M
Symmetrized intensity (arb. units)
Energy relative to E_F (meV)
|Δ| (meV)
T_c = 25.5 K
Temperature (K)

Figure 2

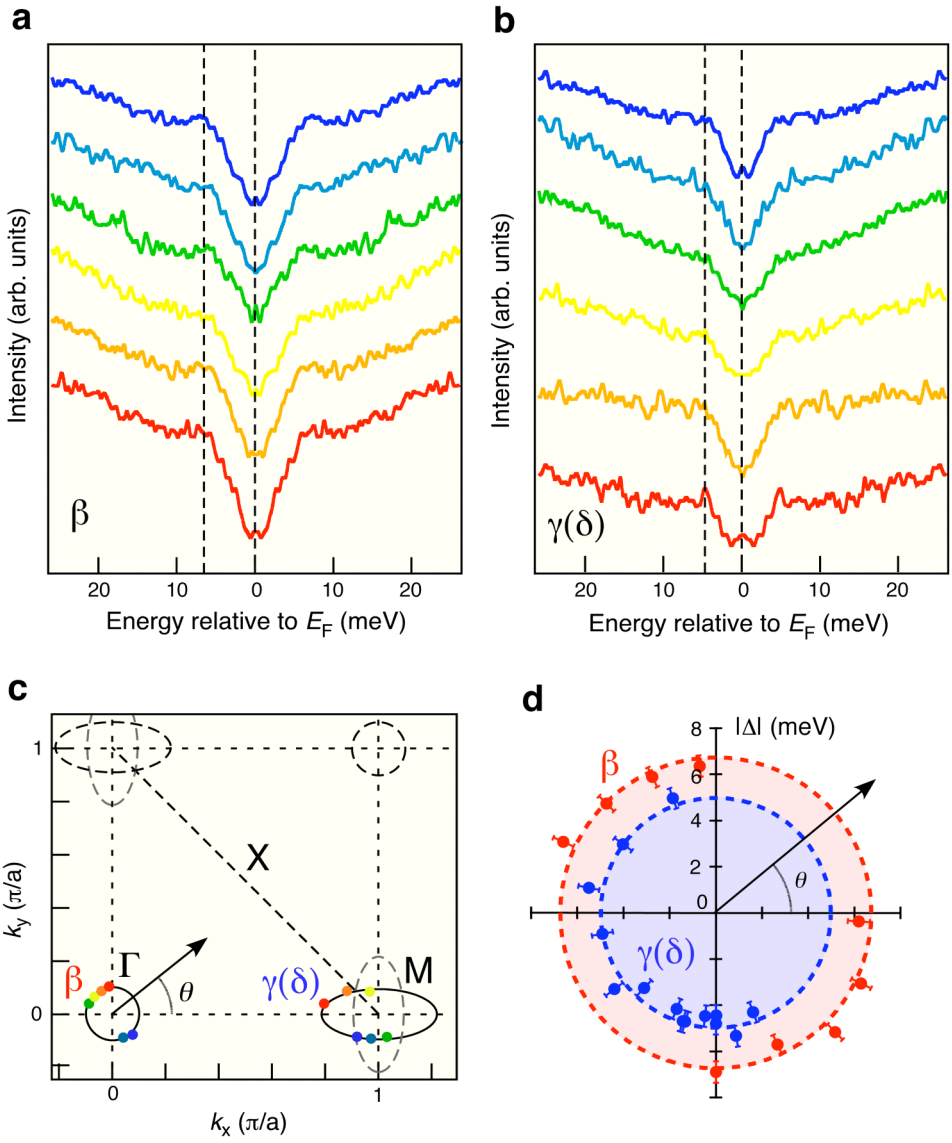
a
b
Intensity (arb. units)
β
γ(δ)
20
10
0
10
20
Energy relative to E_F (meV)
c
d
X
Γ
M
θ
k_y (π/a)
k_x (π/a)
|Δ| (meV)
8
6
4
2
0
1

Figure 3